Petroleum Science 21 (2024) 1865–1874

Contents lists available at ScienceDirect

Petroleum Science

journal homepage: www.keaipublishing.com/en/journals/petroleum-science

Original Paper

A robust viscoelastic surfactant tolerating 20% HCl up to 150 °C for oil well stimulation

Ji Wang [a, b], Ning Qi [c], Hong-Yao Yin [a, *], Yu-Jun Feng [a, **]

[a] Polymer Research Institute, State Key Laboratory of Polymer Materials Engineering, Sichuan University, Chengdu, 610065, Sichuan, PR China
[b] Tianfu Yongxing Laboratory, New Theory and Technology of CO_2 Capture Research Center, Chengdu, 610065, Sichuan, PR China
[c] School of Petroleum Engineering, China University of Petroleum (East China), Qingdao, 266580, Shandong, PR China

ARTICLE INFO

Article history:
Received 15 June 2023
Received in revised form
9 January 2024
Accepted 10 January 2024
Available online 19 January 2024

Edited by Yan-Hua Sun

Keywords:
Viscoelastic surfactants
Thermal stability
Self-diverting acid
Wormlike micelles
Acidizing stimulation

ABSTRACT

Viscoelastic surfactants (VES) are often used as viscous diverters in acidizing stimulation to prolong the acid consumption time and maximize zonal coverage of the acid for improving well productivity. However, the ceiling temperature of commercial VES cannot exceed 120 °C in practical use because of the poor thermal stability and fragile molecular structure, hindering their implementation in high-temperature oil reservoirs, i.e., ≥150 °C. Here we synthesized a novel C_{22}-tailed diamine, *N*-erucamidopropyl-*N*,*N*-dimethylamine (EDPA), and examined comparatively its rheological behavior, assemblies morphology and molecular stability in 20 wt% HCl with a commercial VES, erucyl dimethyl amidopropyl betaine (EDAB). The feasibility of EDPA for acidizing stimulation was assessed by acid etching of carbonate rock with its HCl solution at 150 °C. Rheological results showed that the 2.5 wt% EDPA–20 wt% HCl solution maintains stable viscosity of 90 mPa s at 150 °C for 60 min, while that of 2.0 wt% EDAB HCl solution is just 1 mPa s under identical conditions. ^{1}H NMR spectra and cryo-TEM observations revealed that the chemical structure and self-assembled architectures of EDPA remained intact in such context, but the EDAB suffered from degradation due to the hydrolysis of the amide group, accounting for the poor heat-resistance and acid-tolerance. The reaction rate of 2.5 wt% EDPA HCl solution with carbonate rock was one order of magnitude lower than that of 20 wt% HCl solution at 150 °C, underpinning the potential of EDPA to be used in the high-temperature reservoirs acidizing. This work improved the thermal tolerance of VES in highly concentrated HCl solution, paving a feasible way for the acidization of high-temperature reservoir environments (~150 °C).

1. Introduction

As a fossil fuel with the largest share (31.2%) of global primary energy consumption (Zou et al., 2016), crude oil has been a fundamental engine of technological development, social progress and economic growth. To satisfy enormous oil demand, one feasible avenue is to enhance oil production by acid stimulation of carbonate reservoirs that account for about 70% of the global oil and gas resources and about 50% of the global proved recoverable oil and gas resources (Guo et al., 2020; Abdollahi et al., 2021). However, inherent drawbacks such as inconsistent stimulation of wells (Pourabdollah, 2020; Chacon and Pournik, 2022) and rapid consumption of acid (Chacon and Pournik, 2022) negatively contribute to the efficiency of acidizing stimulation. To tackle this problem, water-soluble polymers (Tian et al., 2020), *in-situ* gelling acid (Ratnakar et al., 2013; Pourabdollah, 2020) and viscoelastic surfactants (VES) (Zhou et al., 2011; Mao et al., 2020; Pourabdollah, 2020; Wanderley Neto et al., 2021) are introduced into the acid solution to control the distribution of acid and retard the acid-rock reaction rate. Compared with the former two systems, the striking advantage of VES is that there is no residue or precipitate to damage the reservoir (Abdollahi et al., 2021). In acidizing, the solution pH and metal ions, mainly Ca^{2+} and Mg^{2+} from calcite and dolomite, increase with acid consumption, inducing the VES monomers to aggregate into wormlike micelles (WLMs), and thus enhancing the viscosity of acid. The high-viscosity acid effectively mitigates the acid–rock reaction and diverts the subsequent acid into the

* Corresponding author.
** Corresponding author.
E-mail addresses: hyyin@scu.edu.cn (H.-Y. Yin), yjfeng@scu.edu.cn (Y.-J. Feng).

https://doi.org/10.1016/j.petsci.2024.01.010

untreated zone, achieving in-depth uniform acidification (Al-Anzi et al., 2003; Abdollahi et al., 2021). More importantly, upon contact with targeted hydrocarbons, the WLMs would disassociate spontaneously, lowering the viscosity and thereby facilitating the removal of spent acid, enabling efficient cleanup (Kefi et al., 2004). During past decades, such clean acid based on VES has been successfully implemented in thousands of carbonate oilwells worldwide and remarkably improved oil production from damaged wells (Nasr-El-Din et al., 2003; Abdollahi et al., 2021).

Nevertheless, existing VES–acid systems are hardly applicable to deep and ultra-deep reservoirs (> 5000 m) where the temperature exceeds 150 °C (Shafiq and Mahmud, 2017; Guo et al., 2020). The reason is that the viscosity of the VES–acid solution deteriorates at elevated temperatures because of the poor thermal stability, undermining the diversion and retarding ability of the acid, resulting in ineffective stimulation. To ensure the successful implementation of the VES–acid solution, as summarized in Table 1, the ceiling temperature of commercial VES (e.g., quaternary ammonium salts of fatty acids (Sullivan et al., 2017) cannot be higher than 120 °C. In principle, the poor heat resistance of VES is associated with the presence of labile bonds including amido-, ester-bond or quaternary ammonium. Upon exposure to high temperatures and aggressive acid environments, these weak bonds would break, causing the decomposition of the molecules. For example, Yu et al. (2012) found the carboxybetaine viscoelastic surfactant, oleamidopropyl dimethyl betaine, in 15 wt% HCl solution undergoes hydrolysis at 76 °C due to the cleavage of the amide bonds. Similarly, high temperature also causes the dealkylation of quaternary ammonium surfactants to form tertiary amines through Hoffmann elimination or nucleophilic substitution (Galimberti et al., 2009). To realize the efficient acidizing treatment of harsh reservoirs (≥150 °C), it is therefore imperative to develop a new VES–acids system that can tolerate high temperatures in strong acids.

To enhance the heat resistance of VES, a common methodology is to introduce nanoparticles, e.g., MgO, SiO_2 and ZnO, into the VES solution (Bybee, 2009; Al-Muntasheri et al., 2017; Philippova and Molchanov, 2019). For instance, Mpelwa and co-workers (Mpelwa et al., 2020) found the binary mixture of 4 wt% sodium 2,2-(propane-1,3-diylbis (stearoylazanediyl))diethanesulfonate (DS18-3-18) and 0.02 wt% MgO could retain a viscosity of 20 mPa s for 120 min at 90 °C at a fixed shear rate of 170 s^{-1}. On the contrary, the viscosity of neat 4 wt% DS18-3-18 aqueous solutions decreases to 5 mPa s under otherwise identical conditions. An analogous result was reported by García and Saraji (2020), who found the zero-shear viscosity of 2.5 wt% tallow alkyl-amido-propyl-dimethyl-amine oxide solution increases from 2700 to 3500 mPa s after adding 0.1 wt% Al_2O_3 at 65 °C. Nevertheless, these studies were carried out in brine or deionized water, it is unclear whether nanoparticles are also applicable in highly concentrated HCl contexts. Furthermore, from the economic perspective, the use of nanoparticles undoubtedly raises the total cost of the VES system, restricting their larger-scale applications in periods of low oil prices.

Another feasible strategy is to optimize the molecular structure of VES, such as lengthening the hydrophobic chain of VES to enhance heat resistance. Plenty of studies demonstrated that the ultra-long tailed VES (hydrophobic tail ≥ C_{18}) such as 3-(*N*-erucamidopropyl-*N,N*-dimethylammonium) propanesulfonate (Chu et al., 2010), erucyldimethylamidopropyl betaine (EDAB) (Kumar et al., 2007), erucylbis-(hydroxyethyl) methylammonium chloride (EHAC) (Kalur et al., 2005; Kwiatkowski et al., 2016) and erucyltrimethylammonium chloride (Raghavan and Kaler, 2001), would present higher viscosity and better heat tolerance compared to their short-chain counterparts, owing to their higher end-cap energy (Raghavan and Kaler, 2001). For instance, Gadberry et al. (2016) reported the viscosity of 4% erucamidopropyl hydroxypropyl sulfobetaine solution can be maintained at 43 mPa s at 135 °C. However, like conventional VES, most ultra-long tailed VES also possess labile bonds including amido-, ester-bond. It can be logically inferred that these ultra-long chain VES also suffer from viscosity loss and degradation under harsh conditions of high temperature and strong acid medium. In this context, we hypothesize that the improved thermal stability of VES in highly acidic environments could be achieved by a novel ultra-long tailed VES without weak bonds.

For this purpose, a novel C_{22}-tailed VES, *N*-erucaminopropyl-*N,N*-dimethylamine (EDPA), with improved chemical stability was designed and engineered. As shown in Scheme 1, the EDPA is structured by the erucyl tail as hydrophobic group and a tertiary

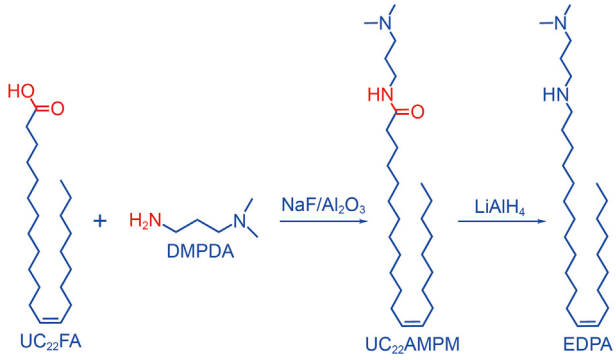

Scheme 1. The pathway towards the synthesis of *N*-erucaminopropyl-*N,N*-dimethylamine (EDPA).

Table 1
The viscosity of acid solutions thickened by VES reported to date.

VES	*T*, °C	C_{VES}, wt%	η, mPa s	C_{HCl}, wt%	$\dot{\gamma}$, s^{-1}	Referebce
TN-16352 anionic surfactant	70	7.5	300	5	100	Czupski et al. (2020)
Oleylamido propyl dimethylamine + *N,N* -dimethyl hexadecyl amine	90	4	50	20	170	Sullivan et al. (2017)
Gemini sulfonated surfactant	120	3	60	4	170	Yu et al. (2012)
Cationic amido propyl quats	90	4	50	15	100	Galimberti et al. (2009)
Betaine-VES	65	6	10	5	100	Czupski et al. (2020)
Sultaine-VES	65	6	300	5	100	Czupski et al. (2020)
Gemini cationic surfactant	120	4	50	20	100	Wang et al. (2012)
3-(*N*-oleamidopropyl-*N,N*-dimethylammonium)propane-sulfonate ($UC_{18}AMP_3SB$)	90	5	90	5	85	Mi et al. (2017)
Gondoyl dimethyl amidopropyl betaine (GDAB)	50	5	/	3.8	/	Bybee (2009)
Gemini zwitterionic viscoelastic surfactant (EDBS)	90	2.1	45	0	170	Al-Muntasheri et al. (2017)
New VES	162	/	/	20	10	Wang et al. (2012)
Erucic amidopropyl betaine	80	3	168	20	170	Mi et al. (2017)

Notes: η is the apparent viscosity of VES–HCl solution; $\dot{\gamma}$ represents the shear rate.

amine as hydrophilic headgroup. The erucyl tail ensures that EDPA features good thickening power and heat resistance, while the tertiary amine head group furnishes it to be thermally stable and insusceptible to degradation. The product was characterized by mass spectrometry (MS), nuclear magnetic resonance (NMR) spectroscopy and high-performance liquid chromatography (HPLC). A commonly used zwitterionic surfactant, EDAB, was chosen as a counterpart for comparative studies in rheological properties, heat resistance, micelle morphology and molecular stability. Finally, static acid-rock reaction test with 2.5 wt% EDPA in 20 wt% HCl solution at 150 °C was performed to demonstrate its application potential.

2. Experimental section

2.1. Materials

Erucic acid (≥ 90%) was provided by Sipo Chemicals (Mianyang, China). *N,N*-dimethyl-1,3-propanediamine (DMPDA, ≥ 98%), lithium aluminumhydride ($LiAlH_4$) (≥ 97%), and $CDCl_3$ (deuterium content, 99.8%) were purchased from Adamas Reagent (Shanghai, China). Hydrochloric acid (HCl, ~36 wt%), sodium fluoride (NaF, ≥ 98%), aluminium oxide (Al_2O_3, ≥ 98%), calcium carbonate ($CaCO_3$, ≥ 98%) and tetrahydrofuran (THF, ≥ 99%) were obtained from Chron Chemicals (Chengdu, China). N_2 (≥ 99.9%) was purchased from Jinnengda Gas Company (Chengdu, China) and was used as received. EDAB was synthesized based on a previously-reported procedure (Feng et al., 2012). Rock samples are obtained from Xinjiang limestone (> 99 wt% $CaCO_3$, Fig. S1 in the Supporting Information) and are cut into disks with a thickness of 8 mm and a diameter of 25 mm. The deionized water with a resistance of 18.25 MΩ cm was obtained using an ultrapure water purification system (CDUPT-III, Chengdu Ultrapure Technology Co., Ltd., China).

2.2. Synthesis of EDPA

As depicted in Scheme 1, EDPA was synthesized via two steps. In the first step, the tertiary amine intermediate ($UC_{22}AMPM$) was prepared following our previously-reported route (Feng and Chu, 2009). The mixture of 15.6 g erucic acid (46.0 mmol) and 7.06 g DMPDA (69.1 mmol) was added to a three-neck round-bottom flask equipped with a condenser. The reaction mixture was refluxed at 155–160 °C under an N_2 atmosphere for 10 h, during which the by-product H_2O was absorbed continuously by anhydrous $CaCl_2$ placed in a solvent still-head distillation apparatus. The resulting solution was cooled down to room temperature. The obtained crude product was purified by recrystallization from a cold mixture of acetone and water (15:1, v/v) to afford 15.0 g of $UC_{22}AMPM$ (yield, 77%). The characterization results of $UC_{22}AMPM$ are shown in Figs. S2 and S3 in the Supporting Information.

In the second step, instead of using the conventional synthetic procedure to modify $UC_{22}AMPM$ (i.e., quaternization reaction), we employed $LiAlH_4$ as a reductant agent to convert the easily hydrolysable amide bond into the robust C–N bond. To be specific, $UC_{22}AMPM$ (12.9 g, 30.5 mmol) was dissolved in 250 mL THF in a round bottom flask equipped with a magnetic stirring bar in an ice water bath. Next, the THF solution of 2.5 M $LiAlH_4$ (40 mL, 100 mmol) was added dropwise to the $UC_{22}AMPM$ solution. The reaction mixture was stirred at 45 °C for 24 h. Upon completion, the reaction mixture was quenched by the sequential dropwise addition of water (50 mL), 15% NaOH aqueous solution (50 mL) and water (50 mL). The resulting suspension was filtered, dried over anhydrous $MgSO_4$ and concentrated *in vacuo* to afford 9.3 g of EDPA as a yellowish oil (yield, 75%).

2.3. Structural characterization

The molecular structure of EDPA was elucidated on an inductively coupled plasma mass spectrometer (ICP-MS, VG PQExcell, UK), and an Avance II spectrometer (Bruker, Switzerland) at 400 and 100 MHz for ^1H and ^{13}C NMR registration.

To check the molecular stability of EDPA or EDAB in HCl solution at 150 °C, the VES–HCl fluids were treated with freezing-drying to extract VES upon completion of the rheological measurement. Then, the recovered VES products were characterized using ^1H NMR and ICP-MS spectrometries as mentioned above.

2.4. Preparation of VES-HCl solution

The designed amount of EDPA or EDAB powder was dissolved in dilute HCl solutions and stirred at 25 °C for 24 h. Then, the obtained homogeneous VES–HCl solution was stored at 25 °C for at least 24 h to reach equilibrium. Acid solutions with different HCl concentrations were prepared by diluting the concentrated HCl stock solution with deionized water.

2.5. Rheological test

The EDPA– and EDAB–HCl solutions were examined separately using an MCR 302 rotational rheometer (Anton Paar, Austria) equipped with a high-pressure and high-temperature cell (PR170/XL) (Fig. S4 in the Supporting Information). The cell made of Hastelloy shows strong tolerance against highly aggressive chemicals, consisting of magnetic coupling, the low friction sapphire based jewel bearings, and a cylindrical measuring cell. Eighteen millilitres of EDPA–HCl or EDAB–HCl solution was placed in the cell and then equilibrated at the desired temperature for no less than 10 min. The pressure was set at 1 MPa to minimize the evaporation of the solvents during measurement. The shear rate ($\dot{\gamma}$) was held at 170 s^{-1} to simulate the shear field to which the acid flow in the porous media, as well as also to obtain enough torque for the accuracy of the measurement.

2.6. Cryogenic transmission electron microscope (cryo-TEM) visualization

The VES–HCl solutions used for cryo-TEM observation were pre-heated to desired temperature (25 or 150 °C) and dropped on a corrosion-resistant carbon-coated gold grid. Then, the grid containing the sample was quenched rapidly in liquid ethane at −183 °C, and next stored in liquid nitrogen at −196 °C. Finally, the vitrified specimens were examined using a Tecnai G2 F20 S-TWIN TEM with an acceleration voltage of 200 kV below −170 °C.

2.7. Static acid–rock reaction

The rotating disk apparatus (Figs. S5(a) and (b) in the Supporting Information) used in this work was manufactured by Hua'an Petroleum Instruments (Hai'an, China). The rock specimen (Figs. S5(c) and (d)) was placed in the disk holder using Teflon tubing and then assembled into the reactor vessel. Afterward, the VES solution was poured into the reservoir vessel and pre-heated to 150 °C. The pressure in the reactor was set at 9 MPa to ensure the generated CO_2 is kept in the solution and does not interfere with the measurement results. Then the rotational speed was set up to 500 rpm to allow the acid solution to be in a laminar flow (Chin and Litt, 2006). During the experiment, 5 mL acid solution was taken at intervals of 2 min to determine the HCl concentration present in the samples using the GT-3000 Potentiometric Titrator (Mettler Toledo, Switzerland). Based on the stoichiometry equation of $CaCO_3$ with

HCl and the measured concentrations, the amount of acid reacted for each sample was determined. From the decrement of acid concentration over time and the initial surface area of the rock sample, the reaction rate could be calculated in units of mol/(cm^2 s).

3. Results and discussion

3.1. Synthesis and characterization of EDPA

As discussed above, the poor heat tolerance of VES may be caused by the cleavage of labile bonds such as amide bonds or ester bonds in their molecule at high temperatures ($\geq$ 120 °C) and highly aggressive conditions. We argued that this issue could be tackled by converting the labile chemical bonds in the molecular structure with robust ones during the preparation process. To confirm the hypothesis, the prepared C_{22}-tailed VES, EDPA, without weak bonds, was synthesized and then examined in hostile conditions. At the same time, one of the currently-used typical VES, EDAB, containing an amide bond was selected to compare with EDPA under identical conditions. To get a more reliable comparison, EDAB was also prepared in the laboratory with high purity following the previously-reported procedure (Chu and Feng, 2012).

As shown in Scheme 1, the EDPA was prepared using erucic acid as a raw material via a two-step process. The erucic acid was first reacted with DMPDA as the amidating reagent to yield the corresponding intermediate ($UC_{22}AMPM$) according to the procedures reported previously (Chu and Feng, 2012). Note that the existence of the amide bond (−CO−NH−) in the $UC_{22}AMPM$ molecule renders it to be hydrolyzed upon exposure to harsh environments. In the second step, we employed $LiAlH_4$ as a reductant to convert the readily hydrolyzable amide bond into the robust C−N bond. ^{1}H NMR (Fig. 1(a)) and ^{13}C NMR (Fig. 1(b)) spectra validated the successful synthesis of EDPA; in particular, the characteristic peak corresponding to carbonyl carbon (C=O) at 173 ppm completely vanishes and a new carbon signal assignable to C−N bond is detected at 48 ppm in the ^{13}C NMR spectrum (Fig. 1(b)), demonstrating the complete transition of the amide bond. Detailed NMR results are listed below:

^{1}H NMR (400 MHz, $CDCl_3$, ppm): δ = 5.56–5.17 (m, J = 3.6 Hz, 2H), 2.76–2.45 (m, 4H), 2.41–2.11 (d, J = 4.1 Hz, 8H), 2.01 (d, J = 4.4 Hz, 2H), 1.65 (d, J = 7.0 Hz, 2H), 1.48 (s, 2H), 1.27 (s, 30H), 0.88 (t, J = 6.4 Hz, 3H).

^{13}C NMR (101 MHz, $CDCl_3$, ppm): δ = 129.8, 62.2, 58.5, 58.0, 50.08, 48.38, 45.47, 45.40, 39.18, 36.9, 32.8, 32.6, 31.9, 30.3, 30.0, 29.7, 29.6, 29.6, 29.6, 29.5, 29.5, 29.5, 29.3, 29.3, 28.0, 27.3, 27.2, 26.1, 25.7, 22.6, 14.1.

The mass-to-charge ratio (m/z = 409.49) in the MS spectrum (Fig. S6 in the Supporting Information) matched well with the theoretical molecular weight ($C_{27}H_{56}N_2$ $[M+H]^+$, m/z = 409.45) of EDPA, further confirming the final product is the targeted EDPA. The purity of the EDPA determined by HPLC is 99.3% (Fig. S7 in the Supporting Information).

3.2. Comparison of thickening power of EDPA and EDAB at 25 °C

As a viscous diverter, the practical use of VES is strongly dependent on the viscosity of its solution. Therefore, it is essential to identify the thickening power of EDPA for evaluating its application potential. Here, 20 wt% HCl solution was employed as a solvent, corresponding to the acid used in the acidizing process where the concentration of HCl solution is typically in the range of 15–28 wt% in practical cases (Abdollahi et al., 2021). The thickening power of both VES in 20 wt% HCl was examined at 25 °C.

It can be observed that both EDAB and EDPA were soluble in HCl solution at 25 °C (the inset of Fig. 2(a)), implying their Krafft temperature (T_k) is less than 25 °C in 20 wt% HCl solution, favoring their end uses in acidizing jobs. The apparent viscosity (η) at 170 s^{-1} of the two solutions rises linearly with increasing concentration (Fig. 2(a)). Note that less EDAB was required than EDPA to achieve a comparable viscosity. For example, the η of 2.0 wt% EDAB is 56 mPa s, to which around 2.5 wt% EDPA is needed. In other words, EDAB shows stronger thickening ability of 20 wt% HCl solution than that of EDPA at 25 °C.

As displayed in the cryo-TEM images, abundant WLMs are evidenced in both 3.0 wt% EDAB–HCl (white arrows in Fig. 2(b)) and 3.0 wt% EDPA–HCl solutions (white arrows in Fig. 2(c)), accounting

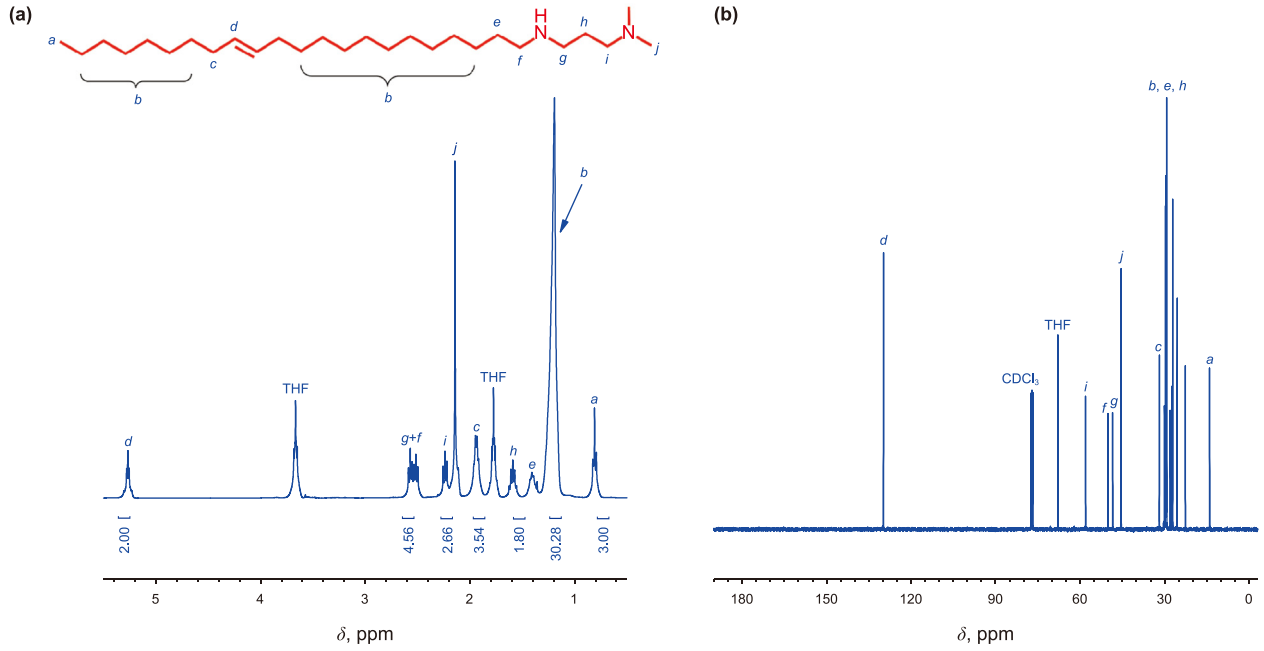

Fig. 1. ^{1}H (**a**) and ^{13}C (**b**) NMR spectra of EDPA in CD_3Cl.

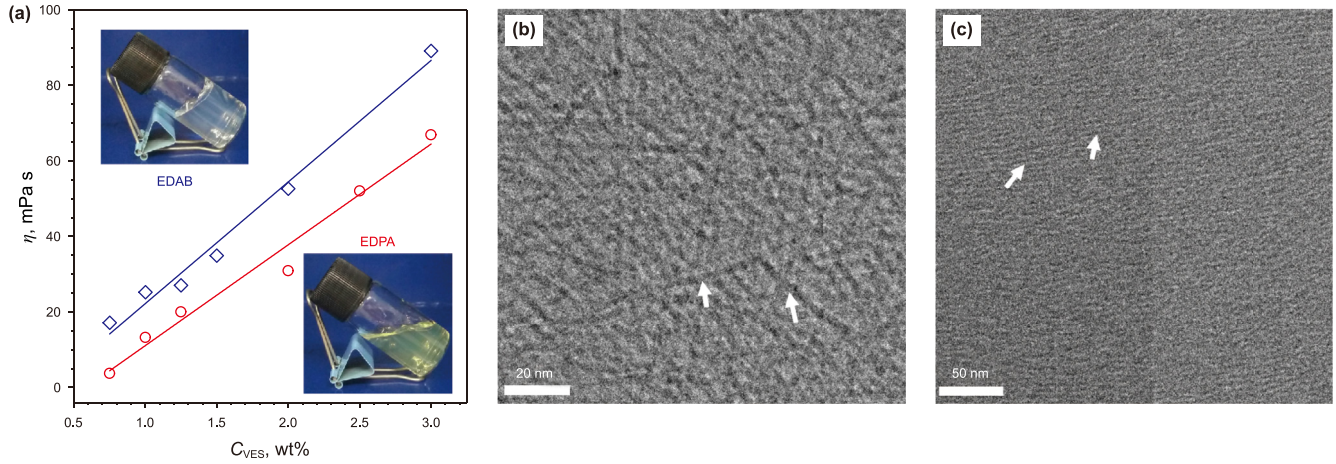

Fig. 2. (**a**) The apparent viscosity (η) of 20 wt% HCl solutions with different concentrations of EDAB and EDPA ($T = 25$ °C, $\dot{\gamma} = 170$ s^{-1}). Inset: snapshots of 3.0 wt% EDAB–HCl and 3.0 wt% EDPA–HCl solutions. Cryo-TEM micrographs of 3.0 wt% EDAB–HCl (**b**) and 3.0 wt% EDPA–HCl (**c**) solutions at 25 °C.

for their good thickening power. It is worth noting that the entanglement density of EDAB WLMs is higher than that of EDPA WLMs, which could explain why EDAB shows a stronger thickening power to HCl solution at 25 °C.

3.3. Thermal stability of VES–HCl solutions at 150 °C

To examine their heat resistance, the rheological behavior of EDPA– and EDA–HCl solutions were compared as a function of temperature at 170 s^{-1}. In this part, the concentration of EDAB and EDPA is fixed at 2.0 and 2.5 wt%, respectively, because of their comparable η at 25 °C and at 20 wt% HCl (Fig. 2(a)). As exhibited in Fig. 3(a), in the case of EDPA–HCl fluid, η initially increases from 60 to around 180 mPa s when the temperature rises from 25 to 110 °C. Such a thermally-induced thickening behavior has also been found previously in long-tailed VES such as *N*-erucamidopropyl-*N,N*-dimethyl-*N*-allyl- ammonium bromide (Wang P. et al., 2017), *N*-erucamidopropyl-*N,N,N*-trimethyl ammonium iodide (Yin et al., 2022), EHAC (Kalur et al., 2005) and EDAB (Wang J. et al., 2017) in aqueous solution. With small-angle neutron scattering and dynamic rheological results, Kalur et al. (2005) and Yin et al. (2022) demonstrated that the elevation η is associated with micellar growth and the enhanced entanglement density of WLMs at lower temperatures. As temperature increases from 100 further to 150 °C, the η decreases from peak viscosity gradually to 130 mPa s. The most likely reason for this is that the contribution of entropy to micellar free energy is more pronounced at higher temperatures, giving rise to an exponential decay of the micellar length (Mukerjee, 1972). The micelles decrease in length, in turn, leads to a decrement of η. It should be pointed out that we tried to examine the EDPA–HCl fluid at higher temperatures (> 150 °C) but found that the high-pressure and high-temperature cell was subjected to corrosion upon temperatures exceeding 150 °C. To avoid apparatus damage, the temperature tested did not exceed 150 °C in the following rheological experiments.

In the case of EDAB–HCl solution, the η also increases firstly and then a sharp decrease upon further increasing temperature. However, two distinctive differences can be evidenced between the two VES systems: first, the transition temperature from thermo-thickening to thermo-thinning appears much earlier for the EDAB system, almost 70 °C ahead that of EDPA solution; second, the final viscosity of EDPA–HCl solution at 150 °C is 130 times of that of the EDAB counterpart at the same temperature, while they have very close starting viscosity at room temperature. Even significantly, the destination viscosity of EDPA–HCl solution doubles its initial one at 25 °C; on the contrary, the final viscosity of EDAB–HCl solution touches the bottom, only 1 mPa s when the temperature reaches 130 °C, just one-sixtieth of the initial viscosity. Such strong contrast in thermal stability suggests the molecular structures of EDAB must have been decomposed, leading to the loss of the thickening ability, but EDPA can remain stable at high temperatures in strong acid media.

To investigate their shear resistance at high temperatures, both solutions were then sheared at 170 s^{-1} for 60 min at 150 °C. Surprisingly, the EDPA–HCl solution can maintain a constant viscosity of approximately 90 mPa s after shearing for 1 h at 150 °C, demonstrating its good thermal stability and shear resistance (Fig. 3(b)). Upon completion of the measurement, the EDPA–HCl solution taken out from the measuring cell kept a transparent viscous state (the inset of Fig. 3(b)), indicative of the significantly improved stability of the EDPA molecular structure.

In the parallel experiment the viscosity curve of the EDAB–HCl solution exhibits considerable fluctuations. When the EDAB–HCl sample was withdrawn, it was found low-viscosity and turbid dispersion, concomitant with the formation of brown paste (the inset of Fig. 3(b)). We proposed that the fluctuation in the viscosity profile is due to the fact that the paste adheres to the measuring bob, causing irregularities in the flow of the solution and consequently fluctuations in the stress. Furthermore, the appearance of phase separation and paste in EDAB–HCl dispersions symbolizes a structural variation of the EDAB molecule.

As exhibited in Fig. 3(c), the WLMs or entangled networks were not formed in the EDAB–HCl system at 150 °C. Combining the TEM observation result in Fig. 2(c), one can conclude that the rapid decay in η of EDAB–HCl solution at 150 °C can be a consequence of the rupture of the WLMs. Instead, three-dimensional networks composed of many WLMs can be found in the EDPA–HCl solution at 150 °C (Fig. 3(d)).

Based on these rheological results, a preliminary conclusion can be drawn that the EDPA–HCl solution possesses better heat resistance and shear tolerance as compared to the EDAB–HCl solution. On the other hand, the differences in micellar structure and appearance of solution reflect the thermal stability of the EDAB molecule in 20 wt% HCl solution at 150 °C is inferior to that of EDPA.

3.4. The mechanism of improved thermal stability

To unravel the underlying reason for the discrepancies in

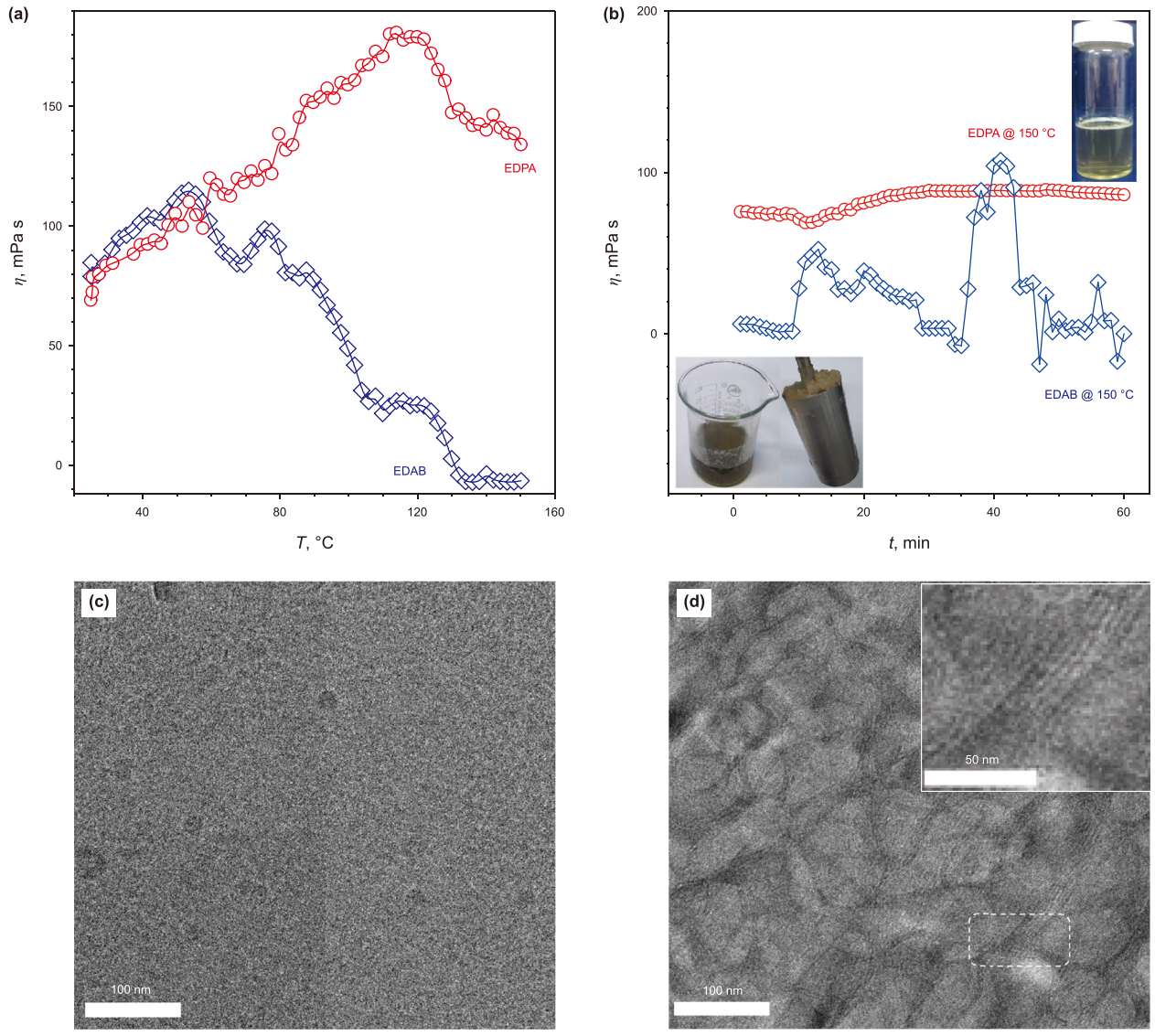

Fig. 3. Apparent viscosity (η) of 2.0 wt% EDAB and 2.5 wt% EDPA in 20 wt% HCl solution plotted as a function of temperature ($\dot{\gamma} = 170\ s^{-1}$) (**a**) and time ($\dot{\gamma} = 170\ s^{-1}$, $T = 150\ °C$) (**b**). Inset: the appearance of the fluid after measurement. Representative cryo-TEM micrographs of 2.0 wt% EDAB–HCl solution (**c**) and 2.5 wt% EDPA–HCl solution (**d**) taken at 150 °C.

thermal stability between EDAB and EDPA, the above two VES–HCl fluids were treated with freezing-drying to extract VES upon completion of the rheological measurement at 150 °C. Afterward, the recovered VES products were characterized using ^{1}H NMR and mass spectrometries.

It can be seen from Fig. 4(a) that the chemical shifts of all protons in CH_2-neighboring amine groups in ^{1}H NMR spectrum of recovered EDPA shifted downfield compared with the spectrum of original EDPA (Fig. 1(a)). The variation in chemical shifts demonstrated that the amine group of EDPA is protonated by HCl, accounting for the increase in solubility of EDPA in HCl solution. It is necessary to mention that other chemical shifts of protons in ^{1}H NMR spectrum of recovered EDPA are consistent with the desired structure, indicating that the molecular structure of EDPA in 20 wt% HCl is robust at 150 °C.

From the MS spectrum of recovered EDPA (Fig. 4(b)), a molecular ion peak ($[M+H]^+$) of 409.47 with high relative intensity was found, which is identical to the spectrum of original EDPA (Fig. S3 in the Supporting Information), and also corresponded well with the theoretical m/z of EDPA (409.45), further demonstrating that EDPA molecules can retain a stable chemical structure in 20 wt% HCl solution at 150 °C; in other words, the EDPA molecules have not been degraded. In summary, EDPA is not subjected to degradation in 20 wt% HCl solutions at 150 °C owing to the absence of weak bonds in its molecular structure, which is the essential reason for the viscosity retention of EDPA–HCl solutions.

Depicted in Fig. 4(c) and (d) are separately the ^{1}H NMR spectra of the recovered solid and liquid part of the EDAB–HCl solution that was sheared at 150 °C. From the ^{1}H NMR spectrum of the solid portion (Fig. 4(c)), the chemical shifts at 1.23, 1.57, 2.00 and 2.21 ppm are assigned to the methylene protons of $-C\mathbf{H}_2-$, $-C\mathbf{H}_2CH{=}CHC\mathbf{H}_2-$, $-C\mathbf{H}_2COO-$, and $-C\mathbf{H}_2CH_2COO-$, respectively. The sharp peak at 0.85 ppm was attributed to the methyl protons of $-C\mathbf{H}_3-$, and the peak at 5.33 ppm represented the alkene protons of $-C\mathbf{H}{=}C\mathbf{H}-$. This suggested that the solid residues correspond to the hydrophobic tail of EDAB.

As for the recovered liquid fraction, the ^{1}H NMR spectrum in Fig. 4(d) displays resonance peaks characteristic of the hydrophilic head group of EDAB, i.e., aminopropyl dimethyl betaine, such as the $-C\mathbf{H}_2-$ at 1.85 ppm, $-NH_2-C\mathbf{H}_2-CH_2-$ at 2.80 ppm, $-C\mathbf{H}_3-N^+-$ at

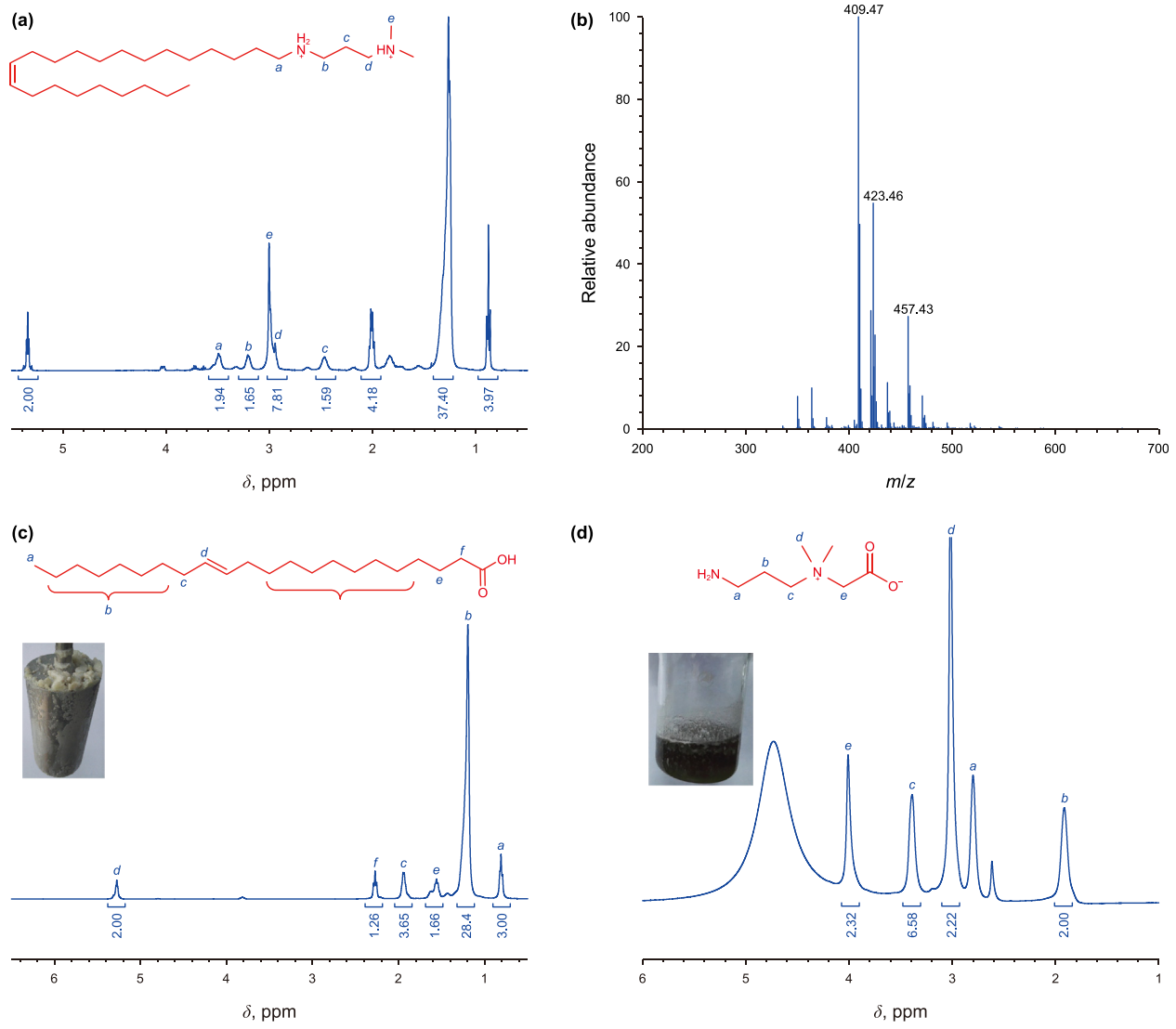

Fig. 4. (**a**) ^{1}H NMR spectrum of recovered EDPA ($CDCl_3$, 400 MHz). (**b**) MS spectrum of recovered EDPA. ^{1}H NMR spectra ($CDCl_3$, 400 MHz) of solid faction (**c**) and liquid portion (**d**) of the EDAB decomposed products.

3.00 ppm, $-CH_2-N^+-$ at 3.30 ppm and $-N^+-CH_2-COO-$ at 4.00 ppm, respectively. These ^{1}H NMR results corroborate that the EDAB molecule hydrolyzed to the precursor of the hydrophobic chain, i.e., erucic acid, and corresponding headgroup, aminopropyl dimethyl betaine in 20 wt% HCl solution at 150 °C. Therefore, the degradation of the EDAB molecules in the HCl solution could be attributed as the root cause for the viscosity decay of the EDAB–HCl solution.

3.5. Retarded acid–rock reaction of EDPA–HCl solution

As stated above, the utilization of VES-based acid solutions for deep oil wells or high-temperature oil reservoirs has always been a considerable challenge. Specifically, the challenge associated with the currently-used VES is the rapid decrease in η because of poor heat resistance, accelerating acid–rock reaction rate and shortening acid penetration distance. In the above sections, we demonstrated that the EDPA in 20 wt% HCl solution could maintain high and stable viscosity (~90 mPa s) at 150 °C for 60 min. Such enhanced thermal stability allows EDPA to be an ideal candidate for acidification in the high-temperature reservoir. To demonstrate the proof of concept, the EDPA–HCl system was further examined by acid etching at 150 °C.

3.5.1. Viscosity evolution during the acid–rock reaction

During the acidizing operation of carbonate minerals, HCl reacts strongly with rock, resulting in a decrease in H^+ concentration as well as an increase in the Ca^{2+} content. It is well established that the concentration of salt affects the self-assembly structures of surfactant, and thus the η of the solution (Han et al., 2011; Das et al., 2012; Wei et al., 2016). Therefore, it is essential to examine the change in η of VES–HCl solution during the acid-rock reaction.

To uncover the evolution in η during the reaction course, different amounts of $CaCO_3$ were added to the 2.5 wt% EDPA–HCl solution to simulate the reaction of HCl with calcite. Then, the samples containing different amounts of HCl and $CaCl_2$ were studied using a rheometer at 150 °C, and the results are given in Fig. 5. Initially, the η of EDPA–HCl solution increases dramatically with increasing Ca^{2+} content, and the maximum value of around 160 mPa s is attained at 5.0 wt% Ca^{2+} loading. The enhanced

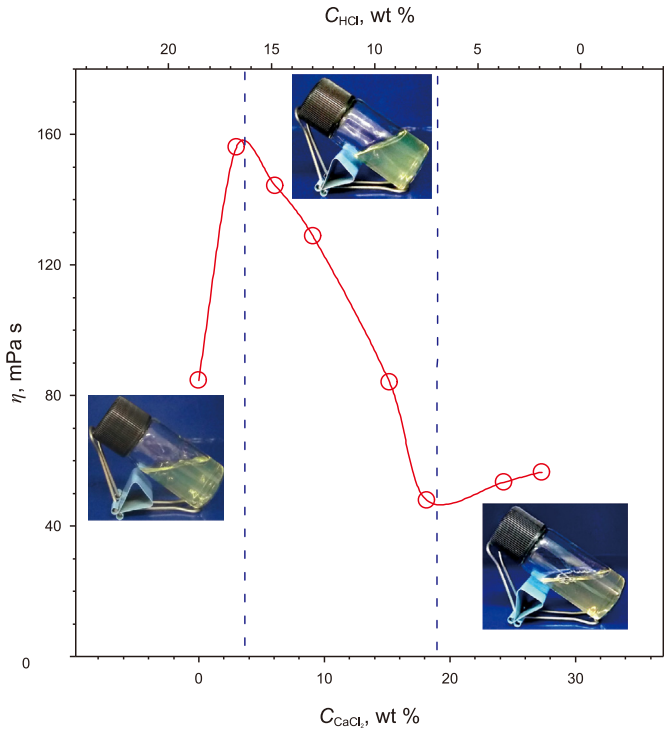

Fig. 5. Change in viscosity (η) for EDPA–HCl solution containing different amounts of HCl and $CaCl_2$ (C_{EDPA} = 2.5 wt%, T = 150 °C, $\dot{\gamma}$ = 170 s^{-1}). The inserts are the photographs of the EDPA–HCl sample after rheological measurements of 2.5 wt% EDPA with different concentrations of HCl: 20 wt% HCl (*left*), 16 wt% HCl solution containing 6.1 wt % $CaCl_2$ (*middle*), 7.4 wt% HCl solution containing 20 wt% $CaCl_2$ (*right*).

viscosity is due to the following fact: (i) The presence of Ca^{2+} decreases the solubility of the hydrophobic chains in water, strengthening the hydrophobic interaction (Ji et al., 2018), leading to the compact packing of the EDPA hydrophobic chains. This process, in turn, promotes the growth and entanglement of WLMs, causing the increment of η. (ii) The Ca^{2+} can coordinate with the N atom of UC_{22}AMPM, leading to cross-linking of the wormlike micellar chains, also enhancing the solution η (Eivazihollagh et al., 2019; Xu et al., 2023). Subsequently, the η decreased slowly with further increasing Ca^{2+} concentration. The reduction in η at high Ca^{2+} concentration can be interpreted with the branching of micelles (Kwiatkowski et al., 2016). When the Ca^{2+} concentration is higher than 20 wt%, the η of fluid remained almost unchanged. The rheological results demonstrate that the EDPA–HCl solution can tune its viscosity automatically during the reaction with rocks, which favors uniform etching of the rock.

3.5.2. Acid–rock reaction rate

It is well recognized that the crucial factor governing the success of the acidizing jobs is the acid–rock reaction rate, which determines the distance that acid can penetrate from the wellbore at a given pumping rate before it is completely spent (Alleman et al., 2003; Liao et al., 2017). Therefore, it is vital to identify the kinetics of the chemical reaction between carbonate and HCl in VES–thickened acid solutions, which provides insightful information, including the rate constant and the reaction order (Zhao et al., 2019).

In fact, the acid–rock reaction rate can be described by acid consumption per unit time (Li et al., 2014). Taking the influence of the area–volume ratio into consideration, the reaction rate can be expressed as (Rabie et al., 2011)

$$J = \frac{\partial C}{\partial t} \cdot \frac{V}{S} \tag{1}$$

where J indicates the reaction rate of HCl with rock, mol/(s cm^2); V denotes acid volume involved in the reaction, L; S represents the surface reaction area of rock, cm^2.

From the results summarized in Table 2, it was seen that the values of J gradually rise with increasing HCl concentration in both cases because more H^+ in the system promotes the reaction rate. Under the otherwise identical condition, the reaction rate of EDPA–HCl solution was significantly less than the 20 wt% HCl solution without EDPA. Combining the rheological properties (Fig. 3(a) and (b)), the deceleration of acid reaction can be rationalized by the high η of the EDPA–HCl fluid, which slows down the rate of diffusion of H^+ from the bulk solution to the surface of the rock.

The acid concentration on the rock surface is assumed to equal the acid concentration in the bulk fluid. In this case, the reaction rate can be expressed as (Lund et al., 1975)

$$J = K \cdot C^m \tag{2}$$

where K represents reaction rate constant, $(mol/L)^{-m}$ mol/(s cm^2); m is the reaction order, dimensionless; C denotes the surface concentration of acid, mole/cm^3. An alternative logarithmic expression of the relationship can be expressed as

$$\lg J = \lg K + m \lg C \tag{3}$$

Using Eq. (3), a function describing the relationship between the reaction rate and the concentration of HCl acid is obtained (Fig. 6(a)). Compared with the reaction rate constant ($K = 3.3 \times 10^{-5}$) of the neat 20 wt% HCl, the K (7.4×10^{-6}) of EDPA–HCl solution is reduced by one order of magnitude, attributed to the reaction rate of EDPA–HCl solution being slower than that of conventional 20 wt% HCl. The reaction order of both EDPA–HCl solution (0.37) and neat 20 wt% HCl (0.72) is less than unity, suggesting that the influence of acid concentration on reaction rate is weak.

The images of the rock after separate treating with EDPA–HCl solution and neat HCl solution are given in Fig. 6(b) and (c). Comparatively, the rock surface after treating with EDPA–HCl fluid is relatively smooth and free of pitting. As for the neat 20 wt% HCl, the rock surface was uneven with a series of pitted holes. This can be explained by the fact that EDPA–HCl fluid could automatically change the η with the acid–rock reaction (Fig. 5), and spontaneously balances the flow of the acid solution, which enables a uniform contact area between H^+ and the rock surface. That is, initially, EDPA–HCl fluids preferentially reacted with high permeability zones of the rock based on the principle of minimum resistance. With the reaction, the η of fluid increased. The high η formed a temporary block zone, hindering fluid flow in the high permeability

Table 2
The acid–rock reaction rate for EDPA–HCl and regular HCl solution at 150 °C.

C_{EDPA}, wt%	C_{HCl}, wt%	V_{HCl}, L	J, mol/(s cm^2)
2.0	5	0.5	8.05×10^{-6}
	10		1.16×10^{-5}
	15		1.25×10^{-5}
	20		4.42×10^{-5}
0	5	0.5	3.98×10^{-5}
	10		8.02×10^{-5}
	15		1.00×10^{-4}
	20		1.12×10^{-4}

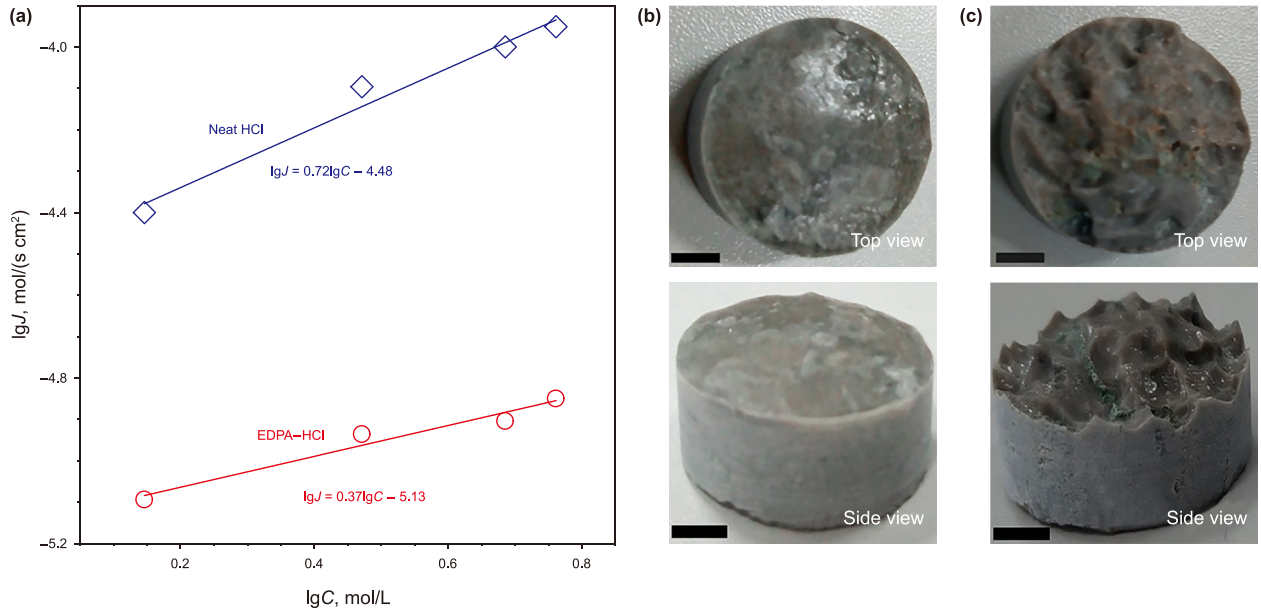

Fig. 6. (**a**) Acid–rock reaction kinetics in EDPA–HCl solution and neat HCl. Core sample after etching with EDPA–HCl solution (C_{EDPA} = 2.5 wt%) (**b**) and neat 20 wt% HCl solution (**c**) at 150 °C. The scale bar is 5 mm.

zone. As a result, the HCl fluid would be forced to enter into the low permeability zone, achieving uniform distribution of acid. Eventually, the entire rock is acidified. Overall, the results demonstrated EDPA has the ability to significantly retard the acid–rock reaction rate and homogenize acidification, evidencing the great potential of the EDPA–HCl system to be used in hostile reservoirs.

4. Conclusions

With the aim of using VES for matrix acidizing in high-temperature oil reservoirs, a structurally robust C_{22}-tailed VES, EDPA, was synthesized from erucic acid through an amidation and reduction reaction. Owing to its robust chemical structure and ultra-long hydrophobic chain, the EDPA molecule remains stable and can self-assemble into WLMs in 20 wt% HCl solution at 150 °C. As a result, 2.5 wt% EDPA–20 wt% HCl solution features high viscosity (~90 mPa s) in such case. More importantly, there is no indication of fatigue in viscosity even after 60 min of steady shearing, mirroring its good thermal stability and acid tolerance. In contrast, the commercial EDAB solution showed a rapid decay in thickening ability under identical conditions, due to the disassembly of WLMs, caused by the decomposition of the EDAB molecule. Compared to commonly used VES, the applicable temperature of EDAP has improved by at least 30 °C at an acidic medium and can reach 150 °C, enabling it to be an attractive candidate for acidizing jobs in high-temperature deep reservoirs.

Indeed, the static acid–rock reaction measurement proved that EDPA could significantly delay the HCl–carbonate rock reaction rate to approximately one order of magnitude in comparison with neat 20 wt% HCl solution at 150 °C, showing good retardation performance. Moreover, the carbonate rock surface after etching by the EDPA–HCl fluid is uniform and smooth, demonstrating homogeneous acidification. This evidence further underpins the potential of EDPA as a thickening agent for acidizing treatment in carbonate formations with high temperatures. Overall, the study engineered a structurally robust VES, EDPA, enhancing the operating temperature of such materials in acidic conditions, broadening their application scope. Furthermore, the comparative results of EDPA and EDAB proved that the cleavage of labile bonds is the root cause of the poor heat tolerance of commercial VES, providing insights into the designing of thermally stable, acid-tolerant VES.

CRediT authorship contribution statement

Ji Wang: Writing – original draft, Methodology, Investigation. **Ning Qi:** Validation, Methodology. **Hong-Yao Yin:** Writing – review & editing, Validation, Methodology, Investigation. **Yu-Jun Feng:** Writing – review & editing, Supervision, Funding acquisition, Conceptualization.

Declaration of competing interest

The authors declare that they have no known competing financial interests or personal relationships that could have appeared to influence the work reported in this paper.

Acknowledgments

The authors would like to thank the financial support from the National Natural Science Foundation of China (Nos: 21773161, 22172108). We acknowledge the Shanghai Office of Anton-Paar company for the provision of high-pressure and high temperatures cell (PR170/XL) for the rheological test. We are also grateful to Dr. Phil Chen and Mr. Zhijiang Wang from Anton-Paar for their critical comments and instructive suggestions on the rheological test.

Appendix A. Supplementary data

Supplementary data to this article can be found online at https://doi.org/10.1016/j.petsci.2024.01.010.

References

Abdollahi, R., Esfandyari, H., Nadri Pari, M., et al., 2021. Conventional diverting techniques and novel fibr-assisted self-diverting system in carbonate reservoir

acidizing with successful case studies. Petroleum Research 6, 247–256. https://doi.org/10.1016/j.ptlrs.2021.01.003.
Al-Anzi, E., Al-Mutawa, M., Al-Habib, N., et al., 2003. Positive reactions in carbonate reservoir stimulation. Oilfield Rev. 15, 28–45. https://doi.org/10.3390/pr10010174.
Al-Muntasheri, G.A., Liang, F., Hull, K.L., 2017. Nanoparticle-enhanced hydraulic-fracturing fluids: a review. SPE J. 186–195. https://doi.org/10.2118/185161-PA.
Alleman, D., Qi, Q., Keck, R., 2003. The development and successful field use of viscoelastic surfactant-based diverting agents for acid stimulation. In: International Symposium on Oilfield Chemistry, pp. 5–7. https://doi.org/10.2118/80222-MS. Houston, Texas, February.
Bybee, K., 2009. Performance improvement of viscoelastic stimulation fluids with nanoparticles. J. Petrol. Technol. 61, 49–50. https://doi.org/10.2118/0609-0049-JPT.
Chacon, O.G., Pournik, M., 2022. Matrix acidizing in carbonate formations. Processes 10, 174–192. https://doi.org/10.3390/pr10010174.
Chin, D.-T., Litt, M., 2006. An electrochemical study of flow instability on a rotating disk. J. Fluid Mech. 54, 613–625. https://doi.org/10.1017/S0022112072000904.
Czupski, M., Kasza, P., Leśniak, Ł., 2020. Development of selective acidizing technology for an oil field in the zechstein main dolomite. Energies 13, 5940–5958. https://doi.org/10.3390/en13225940.
Chu, Z., Feng, Y., Su, X., et al., 2010. Wormlike micelles and solution properties of a C_{22}-tailed amidosulfobetaine surfactant. Langmuir 26, 7783–7791. https://doi.org/10.1021/la904582w.
Chu, Z., Feng, Y., 2012. Vegetable-derived long-chain surfactants synthesized via a "green" route. ACS Sustainable Chem. Eng. 1, 75–79. https://doi.org/10.1021/sc300037e.
Das, N.C., Cao, H., Kaiser, H., et al., 2012. Shape and size of highly concentrated micelles in ctab/nasal solutions by small angle neutron scattering (SANS). Langmuir 28, 11962–11968. https://doi.org/10.1021/la2022598.
Eivazihollagh, A., Svanedal, I., Edlund, E., et al., 2019. On chelating surfactants: molecular perspectives and application prospects. J. Mol. Liq. 278, 688–705. https://doi.org/10.1016/j.molliq.2019.01.076.
Feng, D., Zhang, Y., Chen, Q., et al., 2012. Synthesis and surface activities of amidobetaine surfactants with ultra-long unsaturated hydrophobic chains. J. Surfactants Deterg. 15, 657–661. https://doi.org/10.1007/s11743-012-1359-7.
Feng, Y., Chu, Z., 2009. A facile route towards the preparation of ultra-long-chain amidosulfobetaine surfactants. Synlett 20, 2655–2658. https://doi.org/10.1055/s-0029-1217973.
Galimberti, M., Martino, M., Guenzi, M., et al., 2009. Thermal stability of ammonium salts as compatibilizers in polymer/layered silicate nanocomposites. E-Polymers 9, 1–14. https://doi.org/10.1515/epoly.2009.9.1.686.
García, B.F., Saraji, S., 2020. Linear rheology of nanoparticle-enhanced viscoelastic surfactants. J. Mol. Liq. 300, 112215–112223. https://doi.org/10.1016/j.molliq.2019.112215.
Gadberry, J.F., Engel, M.J., Nowak, J.D., et al., 2016. Thickened viscoelastic fluids and uses thereof. Patent, 9,341,052 B2.
Guo, J., Gou, B., Qin, N., et al., 2020. An innovative concept on deep carbonate reservoir stimulation: three-dimensional acid fracturing technology. Nat. Gas. Ind. 7, 484–497. https://doi.org/10.1016/j.ngib.2020.09.006.
Han, Y., Feng, Y., Sun, H., et al., 2011. Wormlike micelles formed by sodium erucate in the presence of a tetraalkylammonium hydrotrope. J. Phys. Chem. B 115, 6893–6902. https://doi.org/10.1021/jp2004634.
Ji, X., Tian, M., Ma, D., et al., 2018. Effects of calcium ions on the solubility and rheological behavior of a C_{22}-tailed hydroxyl sulfobetaine surfactant in aqueous solution. Langmuir 34, 291–301. https://doi.org/10.1021/acs.langmuir.7b03614.
Kumar, R., Kalur, G.C., Ziserman, L., et al., 2007. Wormlike micelles of a C_{22}-tailed zwitterionic betaine surfactant: from viscoelastic solutions to elastic gels. Langmuir 23, 12849–12856. https://doi.org/10.1021/la7028559.
Kalur, G.C., Frounfelker, B.D., Cipriano, B.H., et al., 2005. Viscosity increase with temperature in cationic surfactant solutions due to the growth of wormlike micelles. Langmuir 21, 10998–11004. https://doi.org/10.1021/la052069w.
Kwiatkowski, A.L., Molchanov, V.S., Orekhov, A.S., et al., 2016. Impact of salt co- and counterions on rheological properties and structure of wormlike micellar solutions. J. Phys. Chem. B 120, 12547–12556. https://doi.org/10.1021/acs.jpcb.6b09817.
Kefi, S., Lee, J., Pope, T., et al., 2004. Expanding applications for viscoelastic surfactants. Oilfield Rev. 16, 10–23.
Liao, Y., Zhang, D., Peng, J., et al., 2017. Measurement of reaction rate of gelled acids and calcite with the rotating disk apparatus. Nat. Resour. 8, 559–568. https://doi.org/10.4236/nr.2017.88035.
Li, N., Feng, Y., Liu, P., et al., 2014. Study of acid–rock reaction kinetics under high temperature and pressure conditions based on the rotating disk instrument. Arabian J. Sci. Eng. 40, 135–142. https://doi.org/10.1007/s13369-014-1504-x.
Lund, K., Fogler, H.S., McCune, C.C., et al., 1975. Acidization—ii. The dissolution of calcite in hydrochloric acid. Chem. Eng. Sci. 30, 825–835. https://doi.org/10.1016/0009-2509(75)80047-9.
Mao, J., Wang, C., Yang, X., et al., 2020. Self-diverting acid system with retarding function for heterogeneous carbonate reservoirs stimulation. J. Surfactants Deterg. 23, 831–839. https://doi.org/10.1002/jsde.12407.
Mi, Q., Li, C., Yi, X., et al., 2017. Novel viscoelastic surfactant-based self-diverting acid systems for carbonate acidizing. Chem. Technol. Fuels Oils 53, 520–528. https://doi.org/10.1007/s10553-017-0831-5.
Mpelwa, M., Zheng, Y., Tang, S., et al., 2020. Performance optimization for the viscoelastic surfactant using nanoparticles for fracturing fluids. Chem. Eng. Commun. 207, 1474–1482. https://doi.org/10.1080/00986445.2019.1660650.
Mukerjee, P., 1972. Size distribution of small and large micelles. multiple equilibrium analysis. J. Phys. Chem. 76, 565–570. https://doi.org/10.1021/j100648a019.
Nasr-El-Din, H.A., Samuel, E., Samuel, M., 2003. Application of a new class of surfactants in stimulation treatments. In: SPE International Improved Oil Recovery Conference in Asia Pacific, Kuala Lumpur, Malaysia, October 20–21. https://doi.org/10.2118/84898-MS.
Philippova, O.E., Molchanov, V.S., 2019. Enhanced rheological properties and performance of viscoelastic surfactant fluids with embedded nanoparticles. Curr. Opin. Colloid Interface Sci. 43, 52–62. https://doi.org/10.1016/j.cocis.2019.02.009.
Pourabdollah, K., 2020. Matrix acidizing: a fouling mitigation process in oil and gas wells. Rev. Chem. Eng. 36, 311–331. https://doi.org/10.1515/revce-2017-0058.
Ratnakar, R.R., Kalia, N., Balakotaiah, V., 2013. Modeling, analysis and simulation of wormhole formation in carbonate rocks with in situ cross-linked acids. Chem. Eng. Sci. 90, 179–199. https://doi.org/10.1016/j.ces.2012.12.019.
Raghavan, S.R., Kaler, E.W., 2001. Highly viscoelastic wormlike micellar solutions formed by cationic surfactants with long unsaturated tails. Langmuir 17, 300–306. https://doi.org/10.1021/la0007933.
Rabie, A.I., Gomaa, A.M., Nasr-El-Din, H.A., 2011. Reaction of in-situ-gelled acids with calcite: reaction-rate study. SPE J. 16, 981–992. https://doi.org/10.2118/133501-PA.
Shafiq, M.U., Mahmud, H.B., 2017. Sandstone matrix acidizing knowledge and future development. J. Pet. Explor. Prod. Technol. 7, 1205–1216. https://doi.org/10.1007/s13202-017-0314-6.
Sullivan, P.F., Panga, M.K.R., Lafitte, V., 2017. Applications of wormlike micelles in the oilfield industry, wormlike micelles: advances in systems, characterisation and applications. The Royal Society of Chemistry 330–352. https://doi.org/10.1039/9781782629788-00330.
Tian, H., Quan, H., Huang, Z., 2020. Investigation on rheological properties and thickening mechanism of a novel thickener based on hydrophobically associating water-soluble polymer during the acid rock reaction. J. Pet. Sci. Eng. 188, 106895–106904. https://doi.org/10.1016/j.petrol.2019.106895.
Wanderley Neto, A.O., da Silva, D.C., Arruda, G.M., et al., 2021. Chemical study of the application of nonionic surfactants nonylphenol in delaying the acidizing reaction of carbonate matrices. J. Dispersion Sci. Technol. 1–8. https://doi.org/10.1080/01932691.2021.1880932.
Wang, G., Nasr-El-Din, H.A., Zhou, J., et al., 2012. A new viscoelastic surfactant for high temperature carbonate acidizing. In: SPE Saudi Arabia Section Technical Symposium and Exhibition, Al-Khobar, Saudi Arabia, April 8–11. https://doi.org/10.2118/160884-MS.
Wang, J., Feng, Y., Agrawal, N.R., et al., 2017a. Wormlike micelles versus water-soluble polymers as rheology-modifiers: similarities and differences. Phys. Chem. Chem. Phys. 19, 24458–24466. https://doi.org/10.1039/C7CP04962E.
Wang, P., Kang, W., Yang, H., et al., 2017b. The *N*-allyl substituted effect on wormlike micelles and salt tolerance of a C_{22}-tailed cationic surfactant. Soft Matter 13, 7425–7432. https://doi.org/10.1039/c7sm01322a.
Wei, X., Geng, P., Han, C., et al., 2016. Rheological properties of viscoelastic solutions in a cationic surfactant–organic salts–water system. Ind. Eng. Chem. Res. 55, 5556–5564. https://doi.org/10.1021/acs.iecr.6b00238.
Yu, M., Mu, Y., Wang, G., et al., 2012. Impact of hydrolysis at high temperatures on the apparent viscosity of carboxybetaine viscoelastic surfactant-based acid: experimental and molecular dynamics simulation studies. SPE J. 1119–1130. https://doi.org/10.2118/142264-PA.
Xu, Z., Yu, S., Fu, R., et al., 2023. pH-responsive viscoelastic fluids of a C_{22}-tailed surfactant induced by trivalent metal ions. Molecules 28, 4621–4634. https://doi.org/10.3390/molecules28124621.
Yin, Q., Tian, Q., Doutch, J., et al., 2022. An insight into the thermo-thickening behavior of wormlike micellar solutions based on ultra-long-chain surfactants. Phys. Chem. Chem. Phys. 24, 11112–11123. https://doi.org/10.1039/d2cp00687a.
Zou, C., Zhao, Q., Zhang, G., Xiong, B., 2016. Energy revolution: from a fossil energy era to a new energy era. Nat. Gas. Ind. 3, 1–11. https://doi.org/10.1016/j.ngib.2016.02.001.
Zhou, F.J., Xiong, C.M., Shi, Y., et al., 2011. Study on a self-diverting acid system for well stimulation based on novel visco-elastic surfactant. Adv. Mater. Res. 287, 3120–3126. https://doi.org/10.4028/www.scientific.net/AMR.287-290.3120.
Zhao, F., Wang, S., Shen, X., et al., 2019. Study on mechanism of gemini surfactant inhibiting acid rock reaction rate. Colloids Surf., A 578, 123629–123634. https://doi.org/10.1016/j.colsurfa.2019.123629.